

See discussions, stats, and author profiles for this publication at: <https://www.researchgate.net/publication/229431027>

Effect of air flow on liquid water transport through a hydrophobic gas diffusion layer of a polymer electrolyte membrane fuel cell

ARTICLE *in* INTERNATIONAL JOURNAL OF HYDROGEN ENERGY · APRIL 2010

Impact Factor: 3.31 · DOI: 10.1016/j.ijhydene.2010.04.052

CITATIONS

16

READS

42

2 AUTHORS, INCLUDING:



Venkata Suresh Patnaikuni

National Institute of Technology, Warangal

6 PUBLICATIONS 46 CITATIONS

[SEE PROFILE](#)



ELSEVIER

Available at www.sciencedirect.comjournal homepage: www.elsevier.com/locate/he

Effect of air flow on liquid water transport through a hydrophobic gas diffusion layer of a polymer electrolyte membrane fuel cell

P.V. Suresh, S. Jayanti*

Department of Chemical Engineering, IIT Madras, Sardar Patel Road, Adyar, Chennai 600036, India

ARTICLE INFO

Article history:

Received 20 February 2010

Received in revised form

9 April 2010

Accepted 11 April 2010

Available online 26 May 2010

Keywords:

Gas diffusion layer

Hydrophobicity

Water management

Two-phase flow

Polymer electrolyte membrane fuel cells

Cross-flow

ABSTRACT

The transport of liquid water through an idealized 2-D reconstructed gas diffusion layer (GDL) of a polymer electrolyte membrane (PEM) fuel cell is computed subject to hydrophobic boundary condition at the fibre–fluid interface. The effect of air flow, as would occur in parallel/serpentine/interdigitated type of flow fields, on the liquid water transport through the GDL, ejection into the channel in the form of water droplets and subsequent removal of the droplets has been simulated. Results show that typically water flow through the fibrous GDL occurs through a fingering and channelling type of mechanism. The presence of cross-flow of air has an effect both on the path created within the GDL and on the ejection of water into the channel in the form of droplets. A faster rate of liquid water evacuation through the GDL (i.e., more frequent ejection of water droplets) as well as less flooding of the void space results from the presence of cross-flow. These results agree qualitatively with experimental observations reported in the literature.

© 2010 Professor T. Nejat Veziroglu. Published by Elsevier Ltd. All rights reserved.

1. Introduction

Effective water management is one of the key issues in the commercialization of low temperature polymer electrolyte membrane fuel cells (PEMFCs). It entails adequate hydration of the proton exchange membrane on one hand and effective evacuation of the excess liquid water on the other. In an operating fuel cell, water is formed as a result of the electrochemical reaction at the catalyst layer on the cathode side; it may also be supplied through the humidified reactant streams. Some of the water is necessary to keep the membrane hydrated; the excess water needs to be evacuated either from the cathode side or from the anode side. In any case, it has to share the flow passage in the gas diffusion layer

(GDL) with gaseous reactants being transported in the opposite direction. At low current densities, the water generation rate may be low enough that it can be evacuated by evaporation. At high current densities, liquid water will be formed and this leads to the formation of a countercurrent two-phase flow of the liquid–gas mixture through the porous gas diffusion layer. Management of this flow is one of the key issues in realizing high current densities from a PEM fuel cell. Generally, the GDL is made of a carbon-based porous medium that allows for the transport of electrons through the fibres and allows the reactants and the liquid water to flow through the void space to/from the catalyst layer. If the evacuation of the liquid water through GDL is not done properly, the pores in the GDL will be filled with water and the flow of the reactants

* Corresponding author. Tel.: +91 4422574168; fax: +91 4422574152.

E-mail address: sjayanti@iitm.ac.in (S. Jayanti).

to the reaction sites will be blocked. The cell performance will then be severely compromised. Studies show that if the carbon fibre medium is coated with an optimum content of polytetrafluoroethylene (PTFE) to make it hydrophobic, then improved cell performance at high current densities can be obtained [1–3]. The objective of the present work is to realize the mechanism of the liquid water transport through a hydrophobic GDL under conditions of practical interest in PEMFC applications in which a fibrous carbon paper is used as the GDL with a parallel/serpentine/interdigitated channel configuration of the gas flow field.

Several numerical and experimental studies have been conducted in recent years on the liquid water transport through the gas diffusion layers and in the flow field channels [4–23] and excellent reviews on the subject have been provided recently [18,24,25]. Liquid water transport through the porous structure is found to be greatly affected by the nature of the porous medium, specifically, its hydrophobicity, which is indicated by the contact angle made by water on the porous medium. The contact angle or the wetting angle is a quantitative measure of the wetting of a solid by a liquid. The actual mechanism of the flow of liquid water through the porous structure is not yet understood clearly. Djilali and Sui [18] presented an overview of transport phenomena in fuel cells from a micro-scale to a macroscale perspective. Kandlikar [24] has presented a comprehensive review of the work done on the water management issues at micro-scale as well as at macro-scale systems level. Bazylak [25] has provided an overview of various experimental visualization techniques and the recent developments in visualizing the liquid water in the PEM fuel cells. Though many visualization studies have been carried out on the behaviour of the liquid water in PEMFCs, the visualization of the flow of water within a GDL porous structure still remains a challenge due to the difficulty in gaining good optical access within the GDL. Two different theories have been proposed by different groups in the literature to describe the water transport mechanism in the gas diffusion layer. Nam and Kavirayani [7] and Pasaogullari and Wang [8] proposed the flow as an ‘upside-down tree’ capillary network, where a large number of small capillaries dispersed evenly within the porous medium converge into larger capillaries and eventually results in one very large capillary that reaches the surface. In contrast, based on their own experimental visualization data, Litster et al. [9] proposed a ‘fingering and channelling’ mechanism for the liquid water transport. They introduced a water-containing fluorescent dye through a small inlet on one face of the GDL and observed the dispersion of water through the microstructure of the porous medium through a microscope. They found that as the water spread through the GDL, numerous dead ends were encountered where the water front receded when an adjacent breakthrough channel formed.

Since the direct visualization of the liquid water transport through the porous gas diffusion layer is difficult, simulating the liquid water transport through the porous medium helps in resolving the microscopic features of the two-phase transport in the GDL. In the present study, direct numerical simulations that explicitly resolve the liquid water transport through a network of fibres representing the GDL is carried out using computational fluid dynamics (CFD) techniques coupled

with the Volume of Fluid (VOF) method [26] for dynamic interface tracking and the Continuum Surface Force (CSF) formulation [27] for surface tension effects.

The Volume of Fluid (VOF) method, which was developed early in 1980s [26] to track gas–liquid interfaces, is widely used for direct numerical simulation of time-dependent flows of immiscible fluids. Recently, these techniques have also been used in the context of fuel cells. The effects of hydrophilic/hydrophobic properties on the water transport behaviour have been studied by Cai et al. [11] by simulating the mobility of water droplets and water films inside a straight micro-channel of a PEMFC using VOF method. They have shown that the removal of water on hydrophobic surface is faster than that on a hydrophilic surface. Theodorakatos et al. [12] investigated computationally and experimentally the detachment of water droplets from carbon porous material surfaces under the influence of an air stream flowing in the flow channel. They used VOF method for predicting the droplet surface deformation and further detachment from different GDL porous surfaces. The liquid water in the above studies [11,12] was assumed to be present in the form of spherical droplets or as film on the GDL surface without considering its emergence from the pore of the GDL. Two-dimensional transient simulations employing VOF method were performed by Zhu et al. [13] to numerically investigate the dynamic behaviour of liquid water entering a flow channel through a GDL pore. The effects of the gas channel size, coalescence of droplets in the channel and pore size on the water droplet dynamics were investigated in their study. They have further extended their study to transient, three-dimensional two-phase flow [14] to investigate the physical mechanism of a water droplet emerging from a GDL pore and performed some numerical experiments to analyze the dynamics of growth, deformation, detachment, motion, coalescence and film formation as a function of wettability of the GDL surface and other operational parameters. All the above mentioned studies have been carried out either from an already placed droplet on the GDL surface or with the droplet emerging from the top surface of the GDL; the transport of the liquid water through the porous space between the banks of fibres in the GDL has not been considered.

Jiao and Zhou [15,16] employed VOF method of formulation to demonstrate the water removal characteristics of the proposed three different kinds of micro-structures of GDLS (different from conventional diffusion layer structure) with a unit serpentine gas flow channel. In these GDL designs, the pores were specifically designed and structured as small holes (such as micro flow channels) connecting the gas flow channel and catalyst layer, which is far different from what prevails in a fibrous GDL medium such as a carbon paper. In all their simulations, an initial constant amount of liquid water distribution was assumed at the bottom of the GDL to determine the water removal characteristics and the effect of electrode wettability on water transport was studied. Djilali [17] and Djilali and Sui [18] presented numerical simulation of liquid water through a 2-D reconstructed structure of a hydrophobic gas diffusion layer and showed the possibility of fingering and channelling mechanism of liquid water transport. In these studies, a constant liquid water reservoir at high pressure was assumed at the bottom of the GDL and the

water transport occurred due to the pressure difference across the GDL. This assumption of constant liquid film/reservoir, which would block the flow of reactants to the active sites for the reaction, corresponds to the extreme case of fully flooded catalyst layer in a PEM fuel cell. Park et al. [19] have modelled a three-dimensional fibrous porous structure to investigate the effect of cross flow on the characteristics of liquid water behaviour in the GDL under the rib area. They considered the GDL to be fully filled with liquid water and performed numerical simulations using the VOF method for a wide range of pressure gradients with different contact angles to determine the minimum pressure gradient that would initiate liquid water transport in the GDL. Numerical simulations using the lattice Boltzmann method (LBM) have also been carried out recently to study the two-phase flow in the gas flow channels and the porous gas diffusion layers [20,21]. Tabe et al. [20] employed LBM to simulate the dynamic capillary fingering at lower migration speeds of liquid water in a reconstructed GDL and also studied the interactions between the liquid water and air flows in the gas flow channels and porous separator.

The present work is directed towards the simulation of the movement of liquid water from the catalyst layer through the GDL into the channel subject to capillary action and internal pressure. Instead of having film/reservoir of liquid water representing the flooded catalyst layer under the GDL, continuous feeding of a small quantity of the liquid water from different places on the bottom surface of the GDL is considered. This corresponds to the situation of liquid water formed at different places in the catalyst layer entering to the gas diffusion layer. The work also focuses on the study of the effect of air flow on the liquid water transport in the GDL and its carryover in the channel as in case of conventional parallel channels. Simulation of the rise and evacuation of liquid water in the presence of cross-flow of air in the GDL as in the case of serpentine and interdigitated flow fields is also considered.

2. Problem formulation and methodology

2.1. Computational geometry and boundary and initial conditions

The flow domain consists of a small, two-dimensional segment consisting of the GDL and channel space, which is a repetitive portion of the total domain in an actual situation. The structure of the GDL is simplified to consist of layers of cylindrical fibres stacked on top of each other. Ten layers, each made up of circular fibres of $8\text{ }\mu\text{m}$ size with a layer-to-layer gap of $1\text{ }\mu\text{m}$ and a fibre-to-fibre gap of $10\text{ }\mu\text{m}$, are considered in the present simulation. The overall size of the computational domain is $196\text{ }\mu\text{m} \times 126\text{ }\mu\text{m}$ with $96\text{ }\mu\text{m}$ height of porous GDL and $30\text{ }\mu\text{m}$ height of flow channel space. The porosity of the reconstructed 2D-GDL structure is 0.74 and the permeability calculated using Carman–Kozeny equation [28] is $5.9 \times 10^{-12}\text{ m}^2$. These dimensions, porosity and the permeability are typical of the values observed in the commonly-used GDLs of PEM fuel cells. An unstructured quadrilateral computational mesh with 122,000 cells is used for the

simulations. Liquid water is introduced continuously at three locations on the bottom face of the GDL, one representing an entry just below a solid fibre, and the other two representing entry in-between two adjacent fibres of the GDL. The circular fibres in the domain are defined as walls with a contact angle of 130° to represent the hydrophobic nature of GDLs. The entire computational domain is initially filled with air, and, at time $t = 0$, liquid water is made to enter the domain from the three inlets at the low velocity of 0.01 m s^{-1} corresponding to a Reynolds number of 0.08 and a capillary number (defined as $\text{Ca} = \mu_L u / \sigma$ where, μ_L is the viscosity of water, u is the velocity and σ is the interfacial tension) of 1.39×10^{-4} which is in the range reported in the literature [20]. An interfacial tension of 0.072 N m^{-1} is used for the water–air interface.

2.2. Computational methodology

The adopted calculation methodology is based on Computational Fluid Dynamics (CFD) simulations in which the fundamental equations governing the flow namely, conservation of mass and conservation of momentum for an unsteady, incompressible flow are solved numerically. The Volume of Fluid (VOF) method has been employed in the present simulations to track the air–water interface in the domain. This models the two immiscible phases by solving a single set of momentum equations and tracking the interface between the phases by solving the continuity equation for volume fraction of one of the phases in each computational cell. This equation for phase q is of the form:

$$\frac{\partial}{\partial t}(\alpha_q \rho_q) + \nabla \cdot (\alpha_q \rho_q \vec{v}_q) = 0 \quad (1)$$

where α_q is the volume fraction of q^{th} fluid in a cell. The velocity field is continuous across the interface, but there is a pressure jump at the interface due to surface tension. The conservation equations governing the unsteady incompressible flow are:

Conservation of mass:

$$\frac{\partial \rho}{\partial t} + \nabla \cdot (\rho \vec{v}) = 0 \quad (2)$$

Conservation of momentum:

$$\frac{\partial}{\partial t}(\rho \vec{v}) + \nabla \cdot (\rho \vec{v} \vec{v}) = -\nabla p + \nabla \cdot [\mu(\nabla \vec{v} + \nabla \vec{v}^T)] + \rho \vec{g} + \vec{F} \quad (3)$$

Here \vec{v} is the velocity, p is the static pressure, ρ and μ are the density and dynamic viscosity, respectively. The fields for all variables (velocity and pressure) and properties (density and viscosity) are shared by the phases. These properties are volume-averaged values, and, for a two-phase air–water system, they are computed from the local value of α_q as

$$\rho = \alpha_2 \rho_2 + (1 - \alpha_2) \rho_1 \quad (4)$$

$$\mu = \alpha_2 \mu_2 + (1 - \alpha_2) \mu_1 \quad (5)$$

The subscripts 1 and 2 represent air and water, respectively.

The force arising out of surface/interfacial tension has been taken into account using the continuum surface force (CSF) formulation of Brackbill et al. [27]. According to this, the source term can be expressed as a function of the surface

tension coefficient of the air–water system, σ_{12} and the surface curvature, k as:

$$\vec{F} = \sigma_{12} \frac{\rho k \nabla \alpha_1}{1/2(\rho_1 + \rho_2)} \quad (6)$$

At a solid surface with a given contact angle (θ), the surface curvature at the interface between the phases is computed from local gradients in the surface normal at the interface as

$$k = \nabla \cdot n = \nabla \cdot (n_w \cos \theta_w + t_w \sin \theta_w) \quad (7)$$

where n is the unit vector normal to the interface between two phases near the wall, n_w is the unit vector normal to the wall, t_w is the unit vector tangential to the wall, and θ_w is the static contact angle at the walls.

All the simulations have been carried out using the commercial CFD package FLUENT version 6.3.26 of ANSYS Inc., USA. All the unsteady simulations have been carried out with a time step of 5×10^{-8} s. The condition that the scaled residuals of all the governing equations are less than 10^{-5} has been used as the convergence criterion in each time step. All the simulations have been carried out in parallel mode with eight quad core CPUs of 16 GB memory. Typically, it took about 20 h of computing time for a real time simulation of 1 m s.

3. Results and discussion

The main forces that are acting on the liquid water transport in the porous GDL are: internal pressure force, which is a resultant of the pressure build up inside the liquid continuum due to the continuous entry of the liquid water (in the present calculation, the pressure appears as a variable in the Navier–Stokes equations); surface tension forces which are resultant of the imbalance of intermolecular attractive forces known as cohesive forces between the molecules (in the present calculation, the surface tension forces are included through the force term \vec{F} given by equation (6)); adhesive forces or wetting forces which are the forces of attraction between the liquid and the solid surface – the difference in strength between the cohesive and adhesive forces determines the behaviour of a liquid water in contact with a solid surface (these are included in the present calculation in the form of contact angle specified at the wall–fluid interface); and shear forces which are resulting from the flow of air which are computed from the velocity gradients and the fluid viscosity.

Calculations of three different cases have been done: (i) rise of liquid water through the GDL as a result of internal pressure, cohesive and adhesive forces; (ii) rise and eventual evacuation of liquid water through the GDL with a cross-current of air flow in the gas distribution channel located above the GDL, which mimics water transport in a conventional parallel gas channel type of flow field; and (iii) rise and evacuation of liquid water in the presence of cross flow of air within the GDL, which mimics the cross-flow conditions encountered under the rib portions of a conventional serpentine and interdigitated flow fields [30]. The results from these calculations are described below. These three cases are summarized schematically in Fig. 1(a)–(c), respectively.

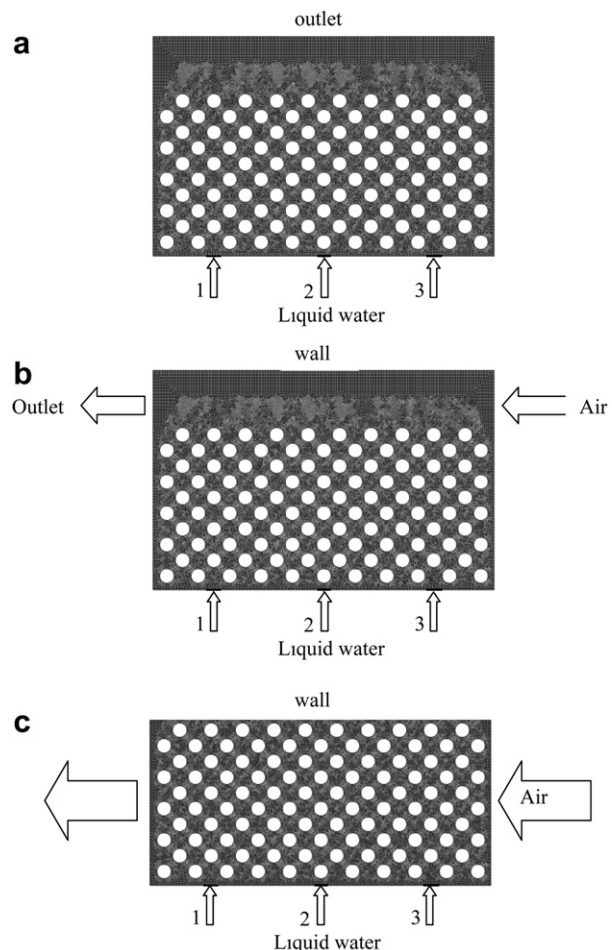


Fig. 1 – Computational domain for the demonstration of liquid water transport in GDL. (a) through capillary fingering and channelling (b) with air flow in parallel channel (c) with cross flow of air under the rib portion of the GDL in case of serpentine/interdigitated channel.

3.1. Liquid water transport in a reconstructed porous GDL

Simulations have been conducted on the reconstructed two-dimensional porous structure as shown in Fig. 1(a) with channel space on top of it. A zero gauge pressure condition is imposed at the top face of the flow domain. This enables air (and water) to flow out through the flow domain and avoids building up of pressure which would occur if the top face was treated as a wall. As mentioned earlier, the inlet water velocity of 0.01 m s^{-1} corresponds to a capillary number of 1.39×10^{-4} is used. The inlets are located such that the distance from the inlet to the nearest fibre (which is hydrophobic with a contact angle of 130°) is different for two inlets (for example, 1 and 2 in Fig. 1(a)) while the conditions are exactly identical to two inlets (1 and 3 in Fig. 1(a)). The transient flow of water through the bank of fibres and the progression of the air–water interface at different times are summarized in Fig. 2. The flow is governed by capillary, viscous forces and the internal pressure is evident from the evolution of the water front.

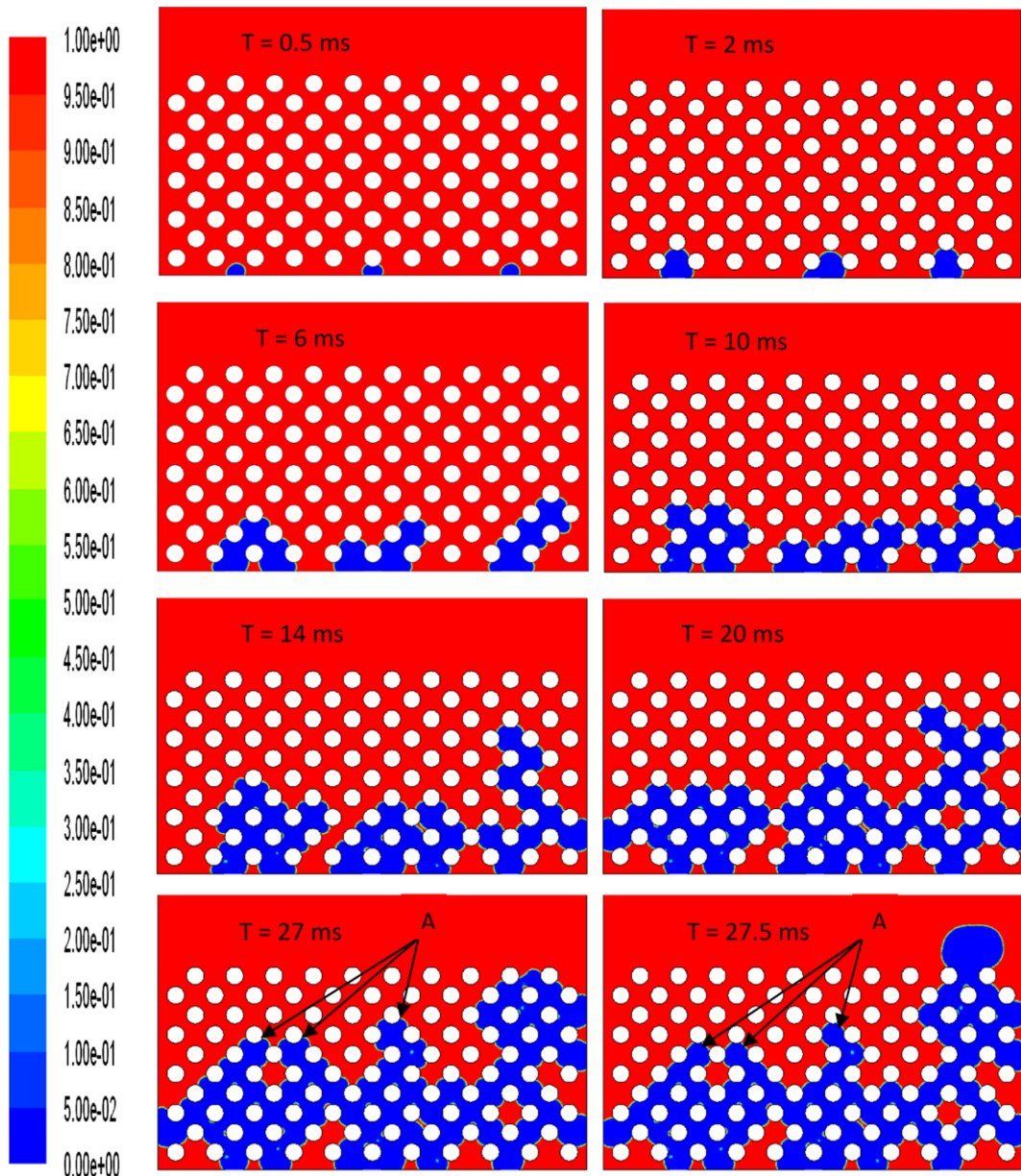


Fig. 2 – Liquid water transport in the hydrophobic GDL with contact angle of 130° with time (blue colour represents liquid water phase and red colour represents air). (For interpretation of the references to colour in this figure legend, the reader is referred to the web version of this article).

Because of the hydrophobic nature of the bottom walls and the fibre walls, the emerging water, instead of spreading laterally, tends to bulge out in the forward direction. The shape of the water drop at 0.5 m s shows the effect of hydrophobicity on the movement of the water within the GDL. By the time of 2 m s, contact with the second set of fibres is made. Lateral spreading of the water film is also evident; however, this arises only because of the interface deformation resulting from the spreading of the water on the first and second layers of fibres. The water from each inlet forms its own pathway which can be likened to fingers. If the paths are close-by, the streams may merge. In such a case, a preferential path is established and more rapid forward movement results in this preferential direction whereas forward movement in the other fingers stops. This results ultimately, by 27 m s in

Fig. 2 by which time water reaches the top row of fibres, in establishing a channel between the inlet (representing the top of the catalyst layer) and the gas flow channel. Further forward movement of the water results in the formation of a large water droplet in the flow channel. Once such breakthrough into the gas channel occurs, further water flow occurs only through that path and further lateral spreading as well as further forward spreading in other “fingers” (labelled as ‘A’ in Fig. 2) is arrested, and flow takes place preferentially through the established channel. Ejection of liquid water in the form of droplet from the diffusion layer/channel interface is observed and the droplet grows bigger and bigger in size with further entry of water. Many visualization experiments [10,22,23] have also suggested the observation of liquid water droplets coming out from the gas diffusion layer into the channel.

The computed variation of pressure at the central inlet (which is typical) with time is shown in Fig. 3. It represents the dynamics of liquid water movement from the bottom surface to the top surface of the GDL and the further water droplet expulsion into the channel. The continuous entering of liquid water increases the pressure at the inlet and makes the water front to bulge out. The changing curvature of the gas–liquid interface has an effect on the surface tension forces which determine by how much the internal pressure on the liquid side of the interface is higher than on the gas phase. Right at the beginning, as the interface becomes curved, the pressure at the inlet increases until it becomes hemispherical. Thereafter, it goes through a series of decreasing and increasing phases. A pressure-decreasing phase occurs when the water progresses through the interstitial spacing between the fibres. The larger radius of curvature in the interstitial spacing leads to a lesser interfacial tension which induces flow in the direction of decreasing radius of curvature. The liquid expands rapidly above this cross-section until the fluid interface contacts an adjacent fibre. At this point, the pressure-increasing phase begins as the interface profile starts adjusting to the contact angle condition at the solid surface and makes progress into the narrowing gap between two adjacent fibres. The pressure keeps increasing with decreasing radius of curvature until the front moves beyond the narrowest gap between two adjacent fibres. In this way the liquid water progresses through the bank of fibres through continual distortion of the water front subjected to hydrodynamic and interfacial forces. At any time, the pressure variation within the liquid continuum is fairly small and the movement of the water front is determined primarily by the contact angle/interface considerations arising out of the irregular geometry of the flow domain. Once the liquid water reaches the GDL-channel interface, further water flow leads to the formation of a water droplet. As it expands freely into the gas channel, the pressure in the liquid continuum decreases rapidly, as is evident in the final stages of the pressure variation shown in Fig. 3. These pressure variations show a remarkable qualitative resemblance to the measured variations reported by Lu et al. [34] and Bazylak et al. [35] in their water breakthrough experiments. The time scales and length scales involved in

those studies and the present study are vastly different and the breakthrough pressures cannot be compared quantitatively. The pressure variations reported in the present study are consistent with the interface curvature and surface tension forces applicable to the present geometry, and fibre dimensions. However, the qualitative agreement is quite encouraging.

Thus, the combination of internal pressure-driven deformation and the capillary action of the wall contact drive the water flow. These simulations match closely with the “fingering and channelling” mechanism of water transport proposed by Litster et al. [8] based on their fluorescence microscopic experimental study. In some cases with low hydrophobic contact angle and in all hydrophilic contact angle cases, no channelling was found to occur and the GDL was uniformly flooded.

3.2. Effect of air on liquid water transport in GDL in a parallel channel flow field

In an actual fuel cell with a parallel channel flow field, air will be flowing in the flow field just above the GDL and, under right conditions, may carry away the water droplets emerging from the GDL. Once liquid water emerges as droplet into the channel, shear forces resulting from the flow over the droplet as well as the pressure difference across the droplet try to deform and move the droplet in the direction of the flow, whereas the surface tension and wetting forces tend to keep the droplet attached to the surface. Liquid water gets carried away when the drag forces exceed the interfacial forces. To demonstrate these effects, the reconstructed GDL computational domain shown in Fig. 1(b) has been used with air inlet at the right side and the pressure outlet at the left side of the channel space (representing the cross section of channel and GDL in the direction along the reactant flow in a parallel channel). Simulations have been carried out on this structure with two different air velocities, namely, 10 and 30 m s⁻¹. These are in the range of velocities that have been used in literature for water droplet evacuation from the flow channel [12–16,34]. Taking a channel hydraulic diameter of 0.7 mm (typical for PEMFC flow fields) and a kinematic

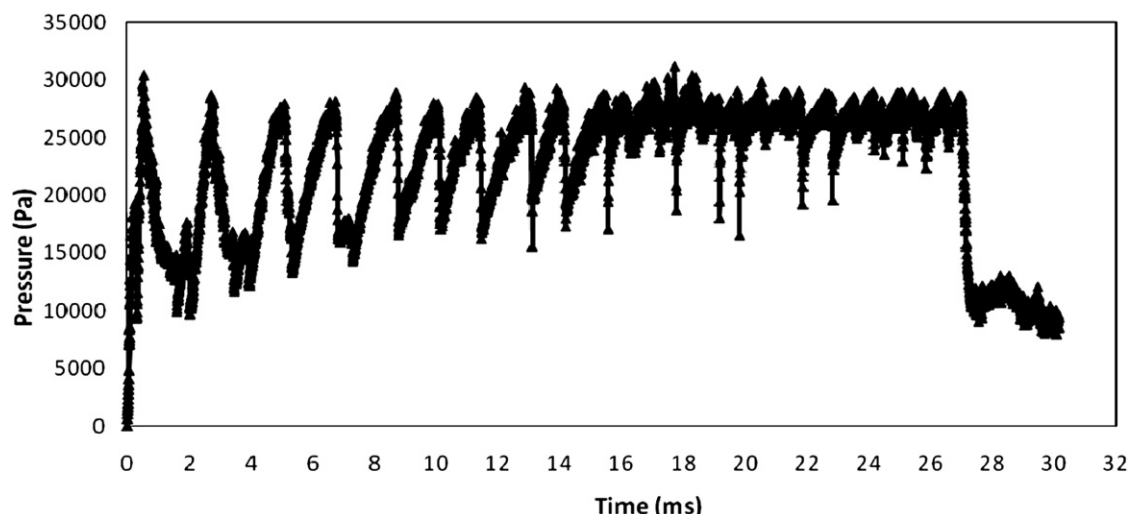


Fig. 3 – Pressure variation at the central inlet during the progress of water through the GDL.

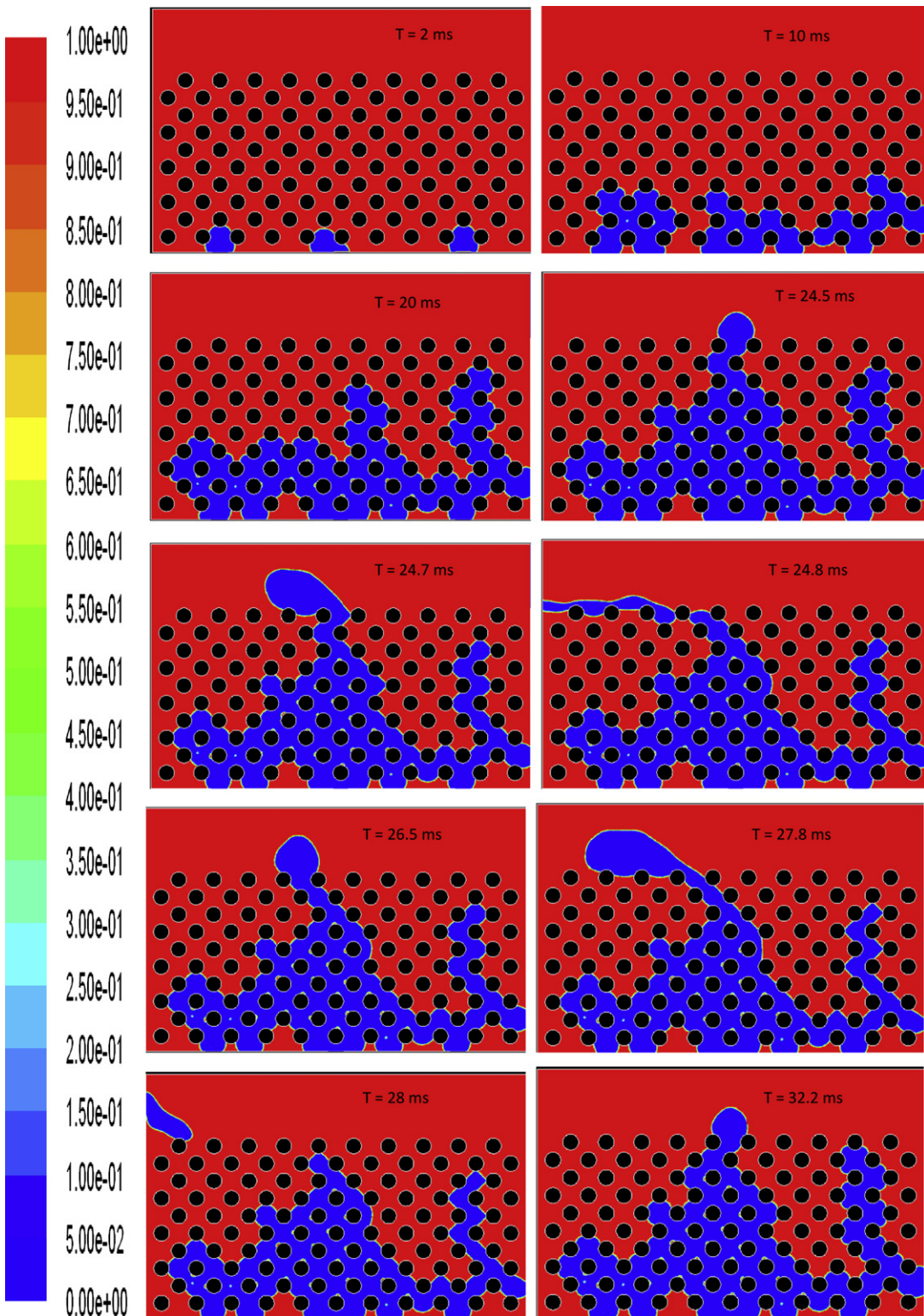


Fig. 4 – Liquid water transport in the hydrophobic GDL with an air flow of 30 m s^{-1} in the gas flow channel (blue colour represents liquid water phase and red colour represents air). (For interpretation of the references to colour in this figure legend, the reader is referred to the web version of this article).

viscosity of air of $1.5 \times 10^{-5} \text{ m}^2/\text{s}$, these velocities correspond to the Reynolds numbers in the range of 466–1400. These are also in the range of Reynolds numbers of 225–4510 used in the experimental investigation on liquid water removal from the GDL by reactant flow in a PEMFC by Jiao et al. [36]. The

high velocity corresponds to the flow rate at higher stoichiometric ratios, which will be normally used at high current densities and under cell flooded condition in the operation of fuel cells. Hence, these air velocities are reasonable in the context of fuel cells operation. The contact

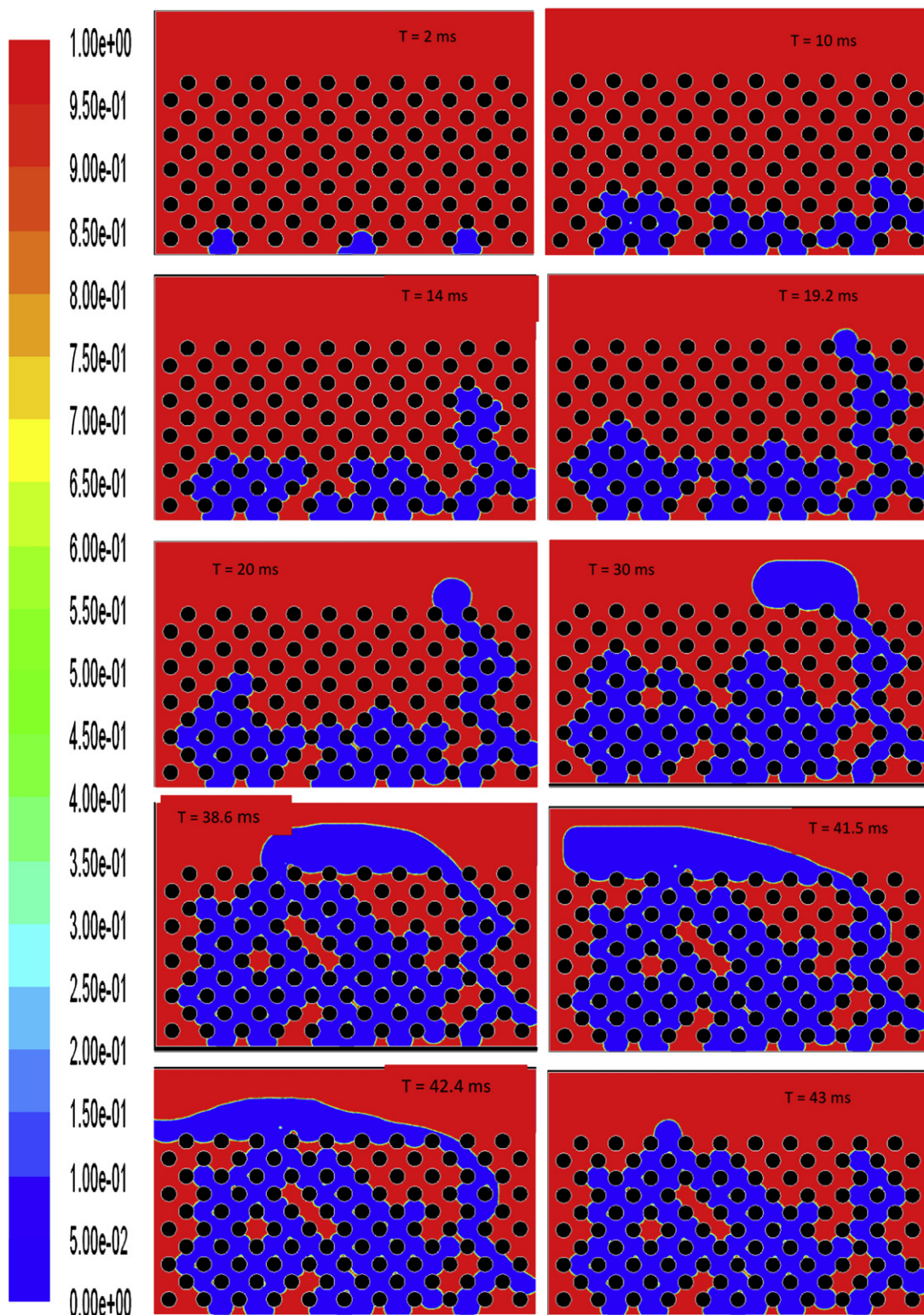


Fig. 5 – Liquid water transport in the hydrophobic GDL with an air flow of 10 m s^{-1} in the gas flow channel (blue colour represents liquid water phase and red colour represents air). (For interpretation of the references to colour in this figure legend, the reader is referred to the web version of this article).

angle and other conditions are the same as those described in Section 3.1.

The transient liquid water progression in the porous GDL with air entering at 30 m s^{-1} is shown in Fig. 4. The liquid water flow develops with the formation of fingers as

described earlier. The air permeating through the porous diffusion medium affects the liquid water flow and leads to the rapid growth of the finger into channel pathway in the middle of the GDL compared to the finger created from the inlet 3. Once the water droplet is ejected into the flow

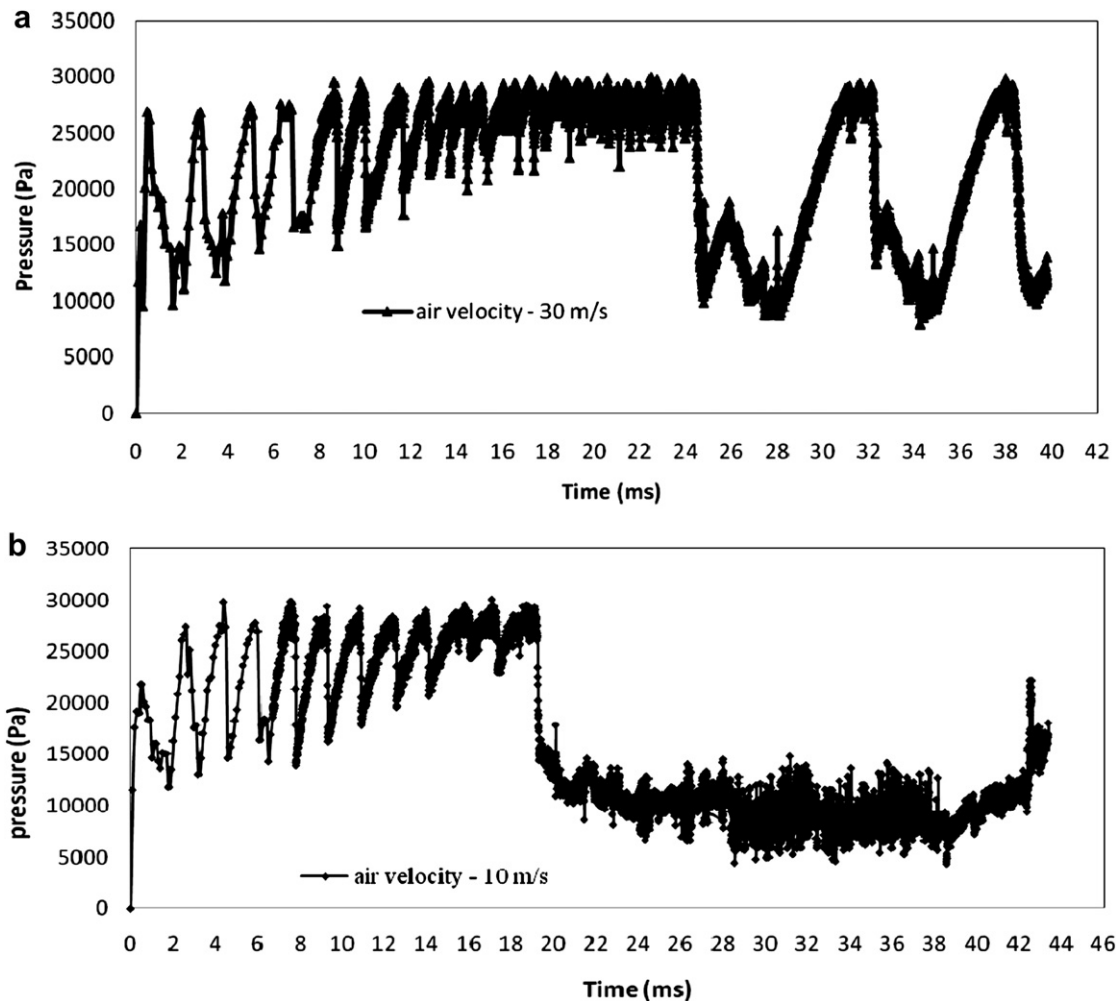


Fig. 6 – Pressure variation at (a) the central inlet with an air flow of 30 m s^{-1} in the gas flow channel (b) the inlet 3 with an air flow of 10 m s^{-1} in the gas flow channel.

channel through the middle channel pathway in GDL (as can be seen in Fig. 4 during 24.5–24.8 ms), the water front recedes in the other fingers and the ejected droplet grows in size with further liquid water flow. During the early stage of the droplet growth, the surface tension and wetting forces dominate and the shape of the droplet remains circular. As time progresses, with the increase in the droplet size, the pressure drop across the droplet increases which destabilizes and deforms the droplet (see the water distribution at a time of 24.7 ms in Fig. 4). Eventually the water droplet breaks off from the fibre and is rapidly carried away by the air flow in the channel. These simulation results are consistent with previous literature on the dynamic behaviour of liquid water droplets [12–14,20,29]. Once the shredding of water takes place, the water surface recedes at the breakthrough point, and, with further flow of water, a new droplet starts growing from the established channel pathway. This droplet again grows very big and eventually gets entrained by the air flow. This process of ejection of liquid water droplet into the flow channel through the gas diffusion medium and its carryover by the entering air occurs periodically as shown in Fig. 4.

The transient liquid water progression in the porous GDL with air entering at 10 m s^{-1} is shown in Fig. 5. The liquid water flow develops with the formation of fingers and channels as described in the earlier section. In this case, the interaction of the permeated air in the GDL with the fingers is less and the finger formed from the inlet 3 is seen developed without merging with other fingers. Hence, the water droplet formation in the channel is seen bit early compared to the previous case, by 19.2 ms and the droplet grows bigger in size with further flow of water. As time progresses, with further flow of water, size of the droplet increases and the pressure drop across the droplet also increases, this destabilizes and deforms the droplet. But it is not sufficient enough to overcome the surface tension force and the wetting force and hence the liquid water forms a film instead of breaking up from the surface. Meantime, the other fingers also have grown up and formed independent channel pathways and eject the droplet into the channel. The water film coming out along the entering air merges with the droplet formed from this finger and forms a big lump of water in the channel. The air pushes this into the outlet and then again new droplet starts coming out from the established channels in the GDL

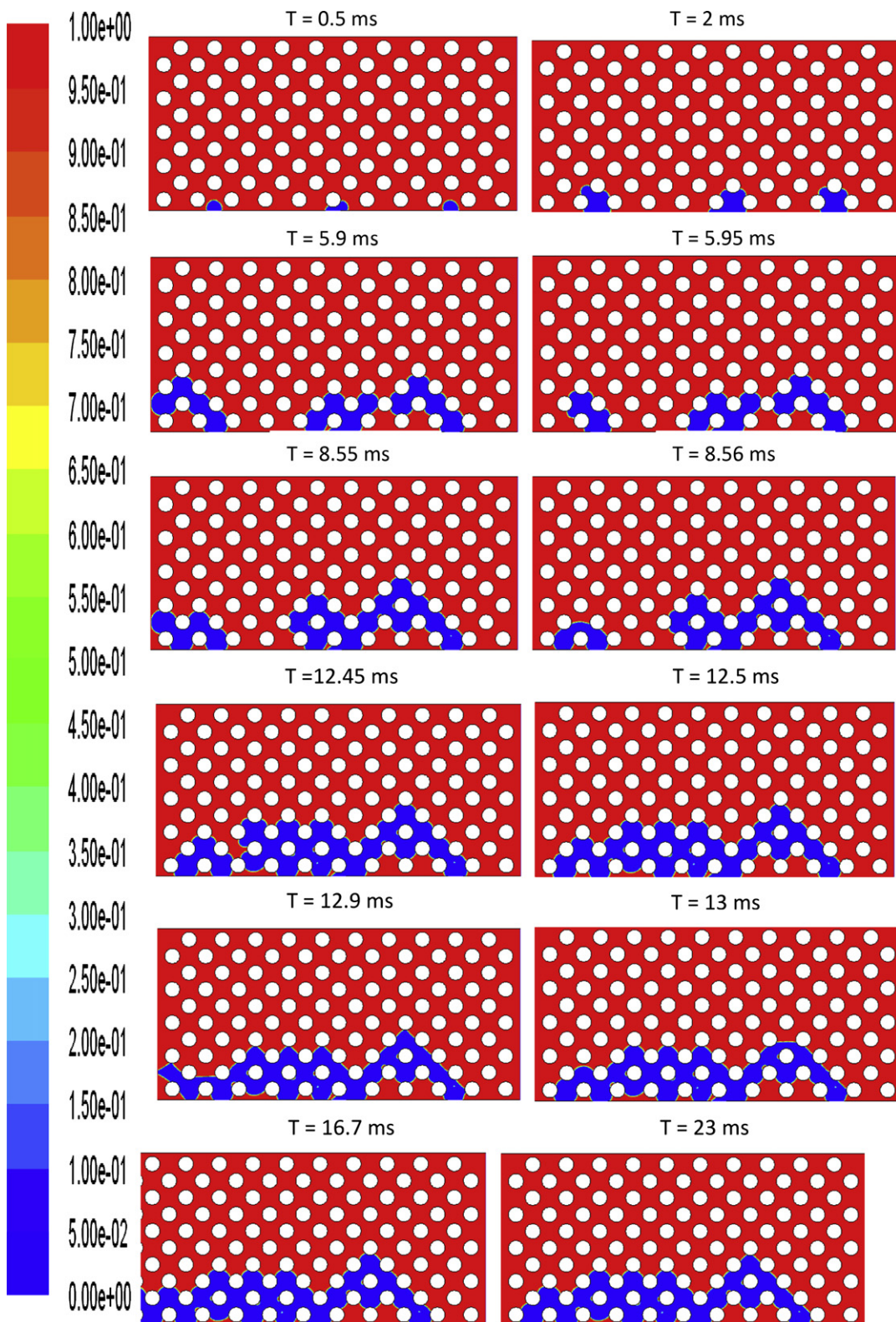


Fig. 7 – Liquid water transport in the under rib portion of the hydrophobic GDL with cross flow of air at 5 m s^{-1} velocity (blue colour represents liquid water phase and red colour represents air). (For interpretation of the references to colour in this figure legend, the reader is referred to the web version of this article).

with further flow of liquid water. Since the entering air velocity is not sufficient enough to break the liquid water from the surface easily, the increasing volume of water in the flow channel causes more blockage of the channel space for

the reactant flow (as observed at 41.5 m s in Fig. 5) and also increases the time for the evacuation of water in the gas channel since its ejection from the GDL (about 42.5 m s in this case).

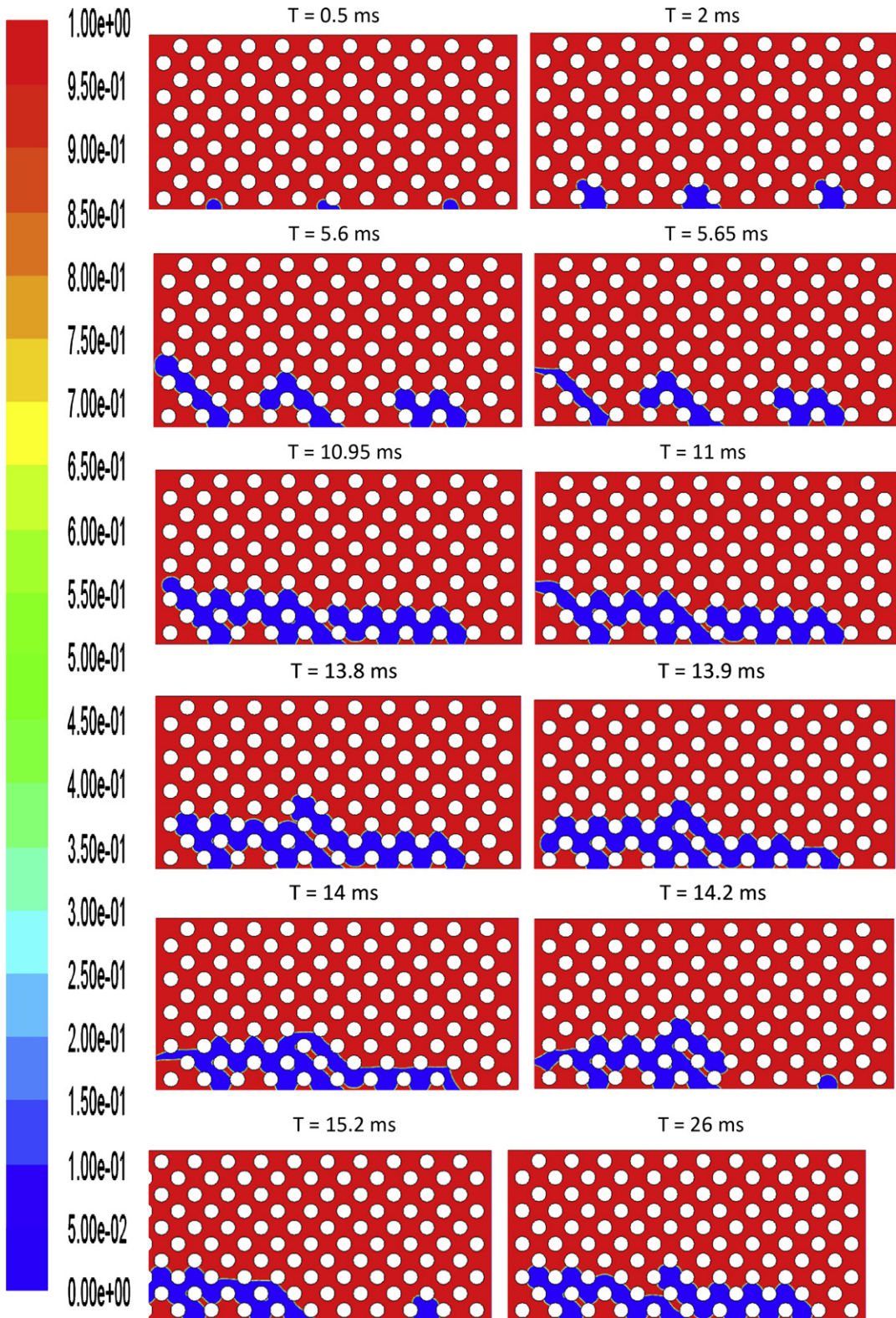


Fig. 8 – Liquid water transport in the under rib portion of the hydrophobic GDL with cross flow of air at 10 m s^{-1} velocity (blue colour represents liquid water phase and red colour represents air). (For interpretation of the references to colour in this figure legend, the reader is referred to the web version of this article).

The pressure variation at the central inlet and inlet 3 of the GDL is shown in Fig. 6(a) and 6(b) for air inlet velocities of 30 ms^{-1} and 10 ms^{-1} , respectively. The inlet pressure variation is similar to that in Fig. 3 as the liquid water progresses through

the GDL by the fingering and channelling process and establishes a flow path to the gas channel. The formation of a large droplet at 24.5 m s leads to a decrease in pressure, which fluctuates over the next 4 m s as it undergoes deformation and

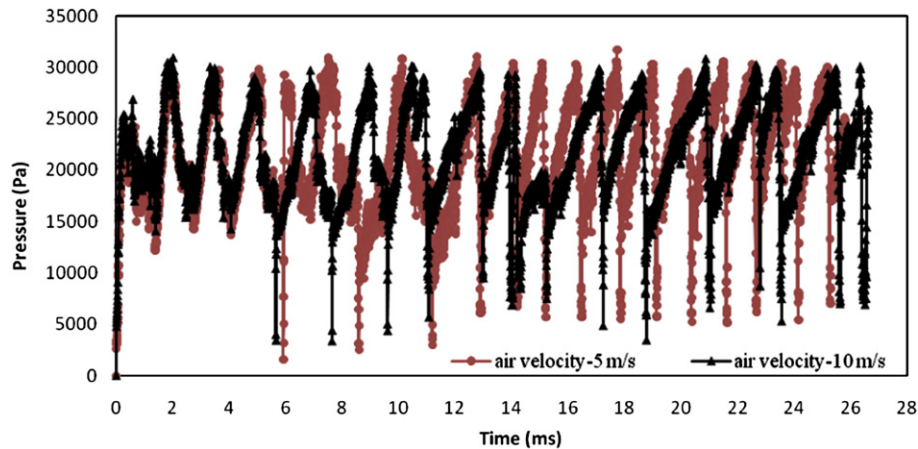


Fig. 9 – Pressure variation at the inlet 1 in the under the rib portion of the hydrophobic GDL with cross flow of air flow at 5 m s^{-1} and 10 m s^{-1} velocity.

eventual shear. In the case of the air velocity of 30 m s^{-1} , the shearing action is strong enough that the liquid water rebounds into the GDL immediately after shear (see Fig. 4, at a time of 28 ms). Water then comes up again to the surface by channelling and proceeds to build up as a large droplet which is again sheared off. Thus, a periodic water droplet growth and ejection happen. When the air flow rate is reduced to 10 m s^{-1} (Fig. 6(b)), the water front reaches the gas channel at a time of about 20 ms resulting in a sudden drop in the inlet pressure at the third inlet. Then it continues at a low pressure level nearly 15 m s as the water is slowly entrained by the air and shows a sudden jump at 42.5 ms at which the drop is sheared off.

Thus, in the presence of cross-flow of air through the gas channel, as would occur in a parallel channel and serpentine flow fields in a PEMFC, periodic drainage of water, in the form of droplets sheared off and regenerated, occurs if the gas velocity is sufficiently high. Present calculations show that a periodic pattern is well-established for a gas velocity of 20 and 30 m s^{-1} but not at 10 m s^{-1} . Taking a channel hydraulic diameter of 0.7 mm (typical for PEMFC flow fields) and the kinematic viscosity of air of $1.5 \times 10^{-5} \text{ m}^2 \text{ s}^{-1}$, the present calculations show that periodic drainage of water occurs for Reynolds numbers of order of 500 or more.

3.3. Liquid water transport in the GDL under the rib portion of serpentine/interdigitated channel in the presence of cross-flow of air

Conventional parallel flow fields transport the reactants and products (water) at a low pressure drop through a diffusion-dominated process. By contrast, a serpentine flow field does this both by diffusion and convection (through cross-flow via the GDL) from one channel to the adjacent one [30,31] but requires a significantly higher pressure drop than the parallel flow field. In an interdigitated flow field, water (liquid or vapour) evacuation from the land area occurs primarily through convection induced by the cross-flow of reactants at an even higher pressure drop than in serpentine flow fields [32,33]. This cross-flow of the reactant through the GDL assists in both the feeding of the reactant and the removal of water

from the catalyst layer. Hence higher current densities can be realized with serpentine and interdigitated flow fields. Simulations of the effect of this type of flow on liquid water transport under the land area of a gas flow field have been carried out using the computational domain shown in Fig. 1(c). Air velocities in the range of $0.5\text{--}10 \text{ m s}^{-1}$ have been used in the simulations to observe the mechanism of water transport in GDL.

Figs. 7 and 8 show the transient water transport in the hydrophobic GDL, which is considered to be under the land area of a typical serpentine/interdigitated flow channel with a cross-flow of air at 5 m s^{-1} and 10 m s^{-1} velocity respectively, entering the computational domain from the right side (as shown in Fig. 1(c)). Liquid water enters the domain from the three inlets provided at the bottom surface of the GDL at a velocity of 0.01 m s^{-1} . The general observations from these figures are as follows: the pressure build up in the liquid continuum during its rise through the porous medium from the inlet is supplemented by the shear force arising from the flow of air around and over it in the cross-wise direction. As a result, the water flow pathways generated in the diffusion medium, instead of rising straight in the forward direction, tend to bend in the direction of air flow. In the process, the pathways created by different liquid water inlets (representing sites on the catalyst layer at which liquid water is generated) merge with the adjacent flow paths and pave a path for the continuous flow of water. If the cross-flow velocity is too high, as in the case of Fig. 8, the pathway may be broken up by shear (as observed from the time of $13.9\text{--}14.2 \text{ ms}$ in Fig. 8) and get reattached later (from 14.2 ms to 26 ms in Fig. 8). This break-up of the pathway does not appear to have taken place at the lower cross-flow velocity case shown in Fig. 7. Results of calculations for lower cross-flow air velocities of 1 and 0.5 m s^{-1} are summarized in Fig. 10. Similar behaviour – such as bending of the pathway in the direction of air flow and subsequent merging of different pathways to form a continuous flow path for water – has also been observed for the low cross-flow velocities. But the fraction of the GDL space that is filled with liquid water is observed to be high for lower cross-flow velocities as the shear force acting on the liquid water pathways is less and hence the liquid water pathways originating from the source points grow to a higher extent compared to the higher velocity case.

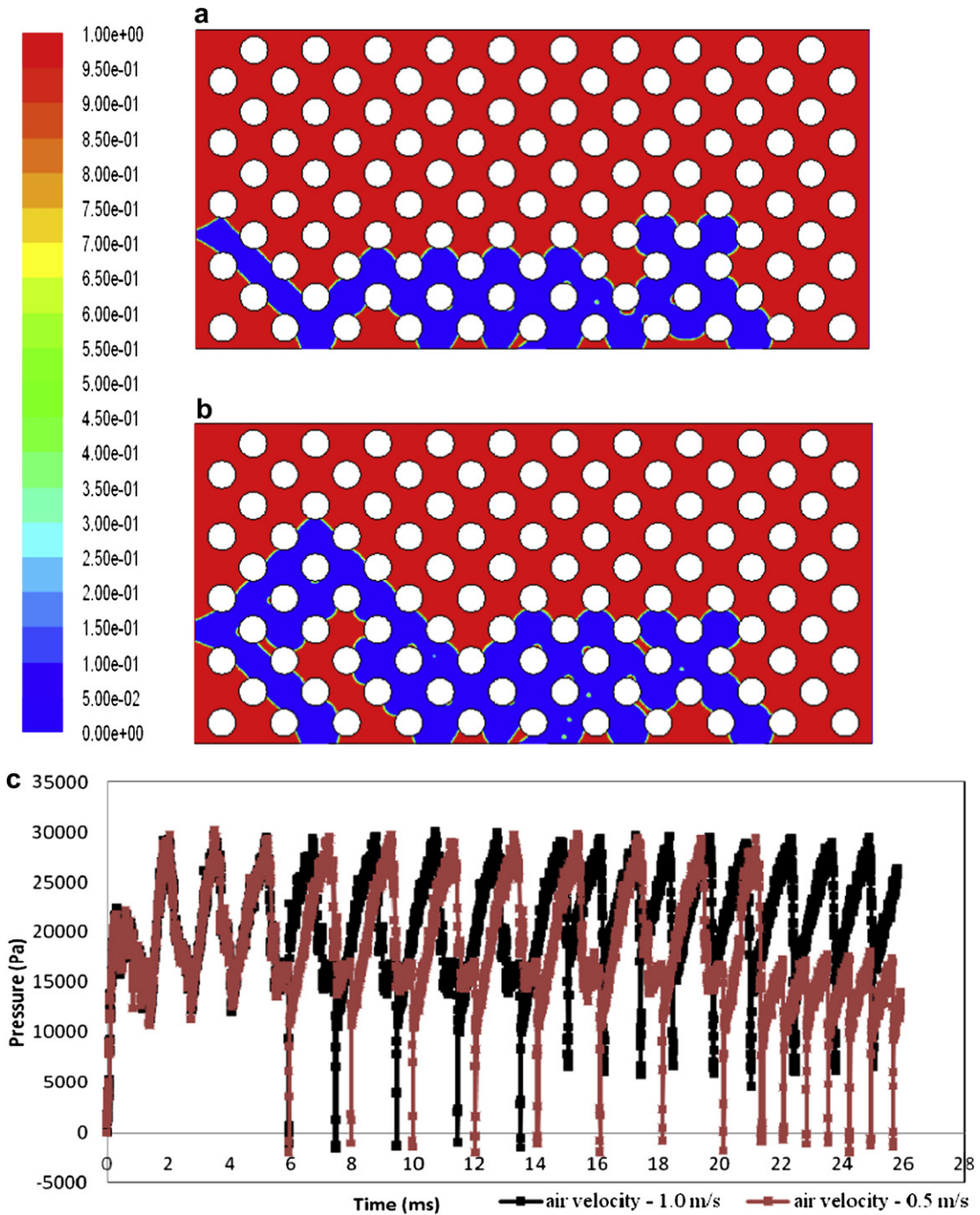


Fig. 10 – Liquid water transport in the under rib portion of the hydrophobic GDL with cross flow of air (a) at 1 m s^{-1} velocity at 21.5 ms (b) with 0.5 m s^{-1} velocity at 22.8 ms (blue colour represents liquid water phase and red colour represents air) (c) pressure variation at the inlet 1 for the cases of (a) and (b). (For interpretation of the references to colour in this figure legend, the reader is referred to the web version of this article).

Thus, the cross flow of reactants or products through the porous medium evacuates liquid water effectively from the GDL without allowing it to spread or fill most of the porous medium, leaving behind more space for the reactant flow, thereby improving the performance of the PEM fuel cell. The intermittent break-up and reattachment of the water path at higher air velocity (Fig. 8) may provide direct access to the catalyst layer surface during the break-up period and may

thereby help in continuing the reaction. It may be noted that a higher cross-flow velocity may evacuate at a higher rate through higher rate of evaporation which is not modelled in the present study.

Fig. 9 shows the pressure variation at the inlet 1 for both the cases of 5 m s^{-1} and 10 m s^{-1} air velocity. The inlet pressure variation undergoes a series of increases and decreases during the liquid water flow through the porous GDL as

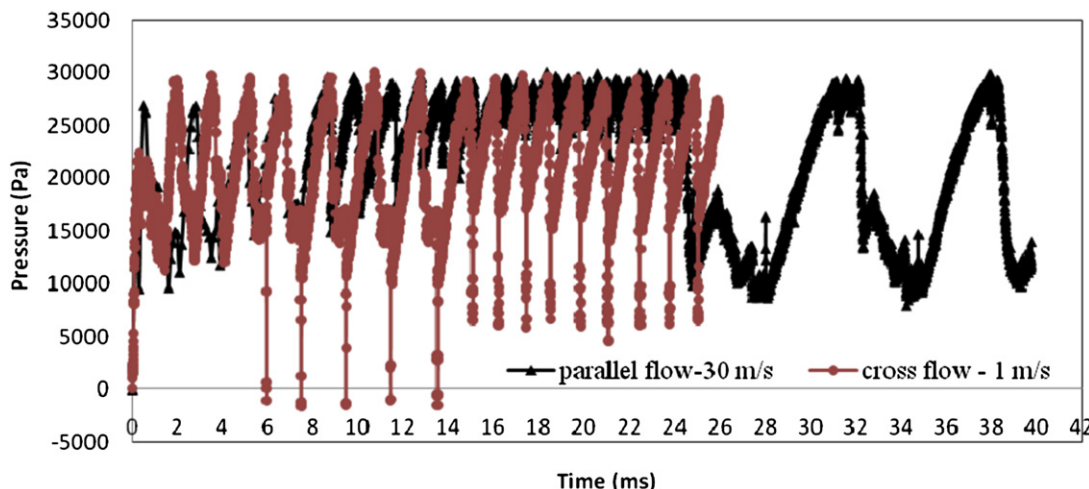


Fig. 11 – Comparison of the pressure variation at the inlet for the parallel flow of air with 30 m s^{-1} velocity and the cross flow of air at 1 m s^{-1} .

discussed earlier. The kinks in the pressure correspond to the release of liquid water to the outlet. As can be seen in Fig. 9, the liquid water release rate is less for low cross flow of air (5 m s^{-1} air velocity) till the continuous liquid water pathway is formed (till 12.9 m s). But, once the continuous pathway is formed, the water release rate is high and occurs more periodically in case of 5 m s^{-1} air velocity, compared to that of 10 m s^{-1} air velocity where the pathway breaks up and forms again. Similar observation can be seen even for low air flow rates such as 1 m s^{-1} and 0.5 m s^{-1} as shown in Fig. 10(c). The time taken for the continuous liquid water pathway to get established is more for lower air flow rates compared to that of higher flow rates. But, once it is formed the water release frequency rate is more for low air flow rates since the water flow path is not disturbed.

Fig. 11 shows a comparison of the pressure profiles at inlet 1 for the parallel flow field at an air flow rate of 30 m s^{-1} and for the serpentine flow field at a cross-flow velocity of 1 m s^{-1} . It can be seen that, while a sustained and periodic ejection of water droplets is present in both cases, the frequency of droplet ejection is more in the latter case, showing the effectiveness of even a small amount of cross-flow in water removal from under the rib area. This would eventually help in delaying the onset of flooding in situations where cross-flow occurs, e.g., in serpentine and interdigitated flow fields.

4. Conclusion

Several calculations have been done to simulate liquid water transport through the GDL under various conditions. These results show that, for sufficiently hydrophobic carbon fibres, thin, preferential channels across the GDL may be formed through which liquid water flows from the site of origin into the gas channel. At the GDL–gas channel interface, the liquid water forms a large droplet which is eventually sheared off and carried away by the gas if the gas velocity is of the order of 10 m s^{-1} or higher. The simulations further show that cross-flow of air through the GDL can lead to a much faster rate (i.e., more

frequent ejection of water droplets) of liquid water evacuation and that considerable portion of the void space is left unflooded. These results confirm the beneficial effects of cross-flow in serpentine and interdigitated flow fields compared to the conventional parallel flow fields in delaying the onset of flooding.

Acknowledgements

The authors gratefully acknowledge the support received from the Department of Science and Technology, India and the High Performance Computing Facility of IIT Madras, India for this work.

Nomenclature

Ca	capillary number
<i>g</i>	acceleration due to gravity, m s^{-2}
<i>n</i>	unit normal vector
<i>p</i>	pressure, Pa
<i>t</i>	time, s
\vec{v}	velocity, m s^{-1}
\vec{F}	force, N

Greek symbols

θ	contact angle, $^\circ$
ρ	density, kg m^{-3}
μ	dynamic viscosity, N s m^{-2}
k	surface curvature, m^{-1}
σ	interfacial tension, N m^{-1}
α	volume fraction

Subscripts

1	fluid 1 (air)
2	fluid 2 (water)
q	fluid, q
w	wall

Abbreviations

CFD	computational fluid dynamics
CSF	continuum surface force
GDL	gas diffusion layer
LBM	lattice boltzmann method
PEM	polymer electrolyte membrane
PEMFC	polymer electrolyte membrane fuel cell
PTFE	polytetrafluoroethylene
VOF	volume of fluid

REFERENCES

- [1] Lin G, Nguyen TV. Effect of thickness and hydrophobic polymer content of the gas diffusion layer on electrode flooding level in a PEMFC. *J Electrochem Soc* 2005;152: A1942–8.
- [2] Velayutham G, Kaushik J, Rajalakshmi N, Dhathathreyan KS. Effect of PTFE content in gas diffusion media and microlayer on the performance of PEMFC tested under ambient pressure. *Fuel Cells* 2007;7:314–8.
- [3] Park GG, Sohn YJ, Yang TH, Yoon YG, Lee WY, Kim CS. Effect of PTFE contents in the gas diffusion media on the performance of PEMFC. *J Power Sources* 2004;131:182–7.
- [4] Owejan JP, Trabold TA, Jacobson DL, Arif M, Kandlikar SG. Effects of flow field and diffusion layer properties on water accumulation in a PEM fuel cell. *Int J Hydrogen Energy* 2007; 32:4489–502.
- [5] Yan WM, Hsueh CY, Soong CY, Chen F, Cheng CH, Mei SC. Effects of fabrication processes and material parameters of GDL on cell performance of PEM fuel cell. *Int J Hydrogen Energy* 2007;32:4452–8.
- [6] Akhtar N, Qureshi A, Scholten J, Hartnig C, Messerschmidt M, Lehnert W. Investigation of water droplet kinetics and optimization of channel geometry for PEM fuel cell cathodes. *Int J Hydrogen Energy* 2009;34:3104–11.
- [7] Nam JH, Kaviany M. Effective diffusivity and water-saturation distribution in single and two layer PEMFC diffusion medium. *Int J Heat Mass Transfer* 2003;46: 4595–611.
- [8] Pasaogullari U, Wang CY. Liquid water transport in gas diffusion layer of polymer electrolyte fuel cells. *J Electrochem Soc* 2004;151:A399–406.
- [9] Litster S, Sinton D, Djilali N. Ex-situ visualization of liquid water transport in PEM fuel cell gas diffusion layers. *J Power Sources* 2006;154:95–105.
- [10] Ous T, Arcoumanis C. The formation of water droplets in an air-breathing PEMFC. *Int J Hydrogen Energy* 2009;34:3476–87.
- [11] Cai YH, Hu J, Ma HP, Yi BL, Zhang HM. Effects of hydrophilic/hydrophobic properties on the water behaviour in the micro-channels of a proton exchange membrane fuel cell. *J Power Sources* 2006;161:843–8.
- [12] Theodorakatos A, Ous T, Gavaises M, Nouri JM, Nikolopoulos N, Yangaihara H. Dynamics of water droplets detached from porous surfaces of relevance to PEM fuel cells. *J Colloid Interface Sci* 2006;300:673–87.
- [13] Zhu X, Sui PC, Djilali N. Dynamic behavior of liquid water emerging from a GDL pore into a PEMFC gas flow channel. *J Power Sources* 2007;172:287–95.
- [14] Zhu X, Sui PC, Djilali N. Three-dimensional numerical simulations of water droplet dynamics in a PEMFC gas channel. *J Power Sources* 2008;181:101–15.
- [15] Jiao K, Zhou B. Innovative gas diffusion layers and their water removal characteristics in PEM fuel cell cathode. *J Power Sources* 2007;169:296–314.
- [16] Jiao K, Zhou B. Effects of electrode wettabilities on liquid water behaviours in PEM fuel cell cathode. *J Power Sources* 2008;175:106–19.
- [17] Djilali N. Computational modelling of polymer electrolyte membrane (PEM) fuel cells: challenges and opportunities. *Energy* 2007;32:269–80.
- [18] Djilali N, Sui PC. Transport phenomena in fuel cells: from microscale to macroscale. *Int J Comput Fluid Dyn* 2008;22: 115–33.
- [19] Park JW, Jiao K, Li X. Numerical investigations on liquid water removal from the porous gas diffusion layer by reactant flow. *Appl Energy* 2010;87:2180–6.
- [20] Tabe Y, Lee Y, Chikahisa T, Kozakai M. Numerical simulation of liquid water and gas flow in a channel and a simplified gas diffusion layer model of polymer electrolyte membrane fuel cells using the lattice Boltzmann method. *J Power Sources* 2009;193:24–31.
- [21] Zhou P, Wu CW. Liquid water transport mechanism in the gas diffusion layer. *J Power Sources* 2010;195:1408–15.
- [22] Kumbar KC, Sharp KV, Mench MM. Liquid droplet behaviour and instability in a polymer electrolyte fuel cell flow channel. *J Power Sources* 2006;161:333–45.
- [23] Su A, Weng FB, Hsu CY, Chen YM. Studies on flooding in PEM fuel cell cathode channels. *Int J Hydrogen Energy* 2006;31: 1031–9.
- [24] Kandlikar SG. Microscale and macroscale aspects of water management challenges in PEM fuel cells. *Heat Transfer Eng* 2008;29:575–87.
- [25] Bazylak A. Liquid water visualization in PEM fuel cells: a review. *Int J Hydrogen Energy* 2009;34:3845–57.
- [26] Hirt CW, Nichols BD. Volume of Fluid (VOF) method for the dynamics of free boundaries. *J Comput Phys* 1981;39: 201–25.
- [27] Brackbill JU, Kothe DB, Zemach C. A continuum method for modeling surface tension. *J Comput Phys* 1992;100: 335–54.
- [28] Gostick JT, Fowler FM, Pritzker MD, Ioannidis MA, Behra LM. In-plane and through-plane gas permeability of carbon fiber electrode backing layers. *J Power Sources* 2006; 162:228–38.
- [29] Golpayagan A, Ashgriz N. Multiphase flow model to study channel flow dynamics of PEM fuel cells: deformation and detachment of water droplets. *Int J Computat Fluid Dyn* 2008; 22:85–95.
- [30] Shyam Prasad KB, Jayanti S. Effect of channel-to-channel cross-flow on local flooding in serpentine flow-fields. *J Power Sources* 2008;180:227–31.
- [31] Park J, Li X. An experimental and numerical investigation on the cross flow through gas diffusion layer in a PEM fuel cell with a serpentine flow channel. *J Power Sources* 2007;163: 853–63.
- [32] Shyam Prasad KB, Suresh PV, Jayanti S. A hydrodynamic network model for interdigitated flow fields. *Int J Hydrogen Energy* 2009;34:8289–301.
- [33] Li X, Sabir I. Review of bipolar plates in PEM fuel cells: flow-field designs. *Int J Hydrogen Energy* 2005;30:359–71.
- [34] Lu Z, Daino MM, Rath C, Kandlikar SG. Water management studies in PEM fuel cells, part III: dynamic breakthrough and intermittent drainage characteristics from GDLs with and without MPLs. *Int J Hydrogen Energy* 2010;35:4222–33.
- [35] Bazylak A, Sinton D, Djilali N. Dynamic water transport and droplet emergence in PEMFC gas diffusion layers. *J Power Sources* 2008;176:240–6.
- [36] Jiao K, Park J, Li X. Experimental investigations on liquid water removal from the gas diffusion layer by reactant flow in PEM fuel cell. *Appl Energy*; 2009; [doi:10.1016/j.apenergy.2009.04.041](https://doi.org/10.1016/j.apenergy.2009.04.041).